Spora: A Journal of Biomathematics

Volume 10 Article 8

2024

Improved Efficiency and Sensitivity Analysis of 3-D Agent-based Model for Pain-related Neural Activity in the Amygdala

Kayla Kraeuter
Duquesne University, kraeuterk@duq.edu

Carley Reith
Duquesne University, crreith5@gmail.com

Benedict J. Kolber
University of Texas at Dallas, benedict.kolber@utdallas.edu

Rachael Miller Neilan
Duquesne University, millerneilanr@duq.edu

Recommended Citation

Kraeuter, Kayla; Reith, Carley; Kolber, Benedict J.; and Miller Neilan, Rachael (2024) "Improved Efficiency and Sensitivity Analysis of 3-D Agent-based Model for Pain-related Neural Activity in the Amygdala," *Spora: A Journal of Biomathematics*: Vol. 10, 65–82.
DOI: https://doi.org/10.61403/2473-5493.1094
Available at: https://ir.library.illinoisstate.edu/spora/vol10/iss1/8

Intercollegiate Biomathematics Alliance

SPORA
A Journal of Biomathematics

ISSN 2473-3067 (Print)
ISSN 2473-5493 (Online)

Improved Efficiency and Sensitivity Analysis of 3-D Agent-based Model for Pain-related Neural Activity in the Amygdala

Kayla Kraeuter[1,2], Carley Reith[1], Benedict J. Kolber[3], Rachael Miller Neilan[1,*]

*Correspondence:
Dr. Rachael Miller Neilan,
Dept. of Mathematics and Computer Science, Duquesne University, 600 Forbes Ave, Pittsburgh, PA 15282, USA
millerneilanr@duq.edu

Abstract

Neuropathic pain is caused by nerve injury and involves brain areas such as the central nucleus of the amygdala (CeA). We developed the first 3-D agent-based model (ABM) of neuropathic pain-related neurons in the CeA using NetLogo3D. The execution time of a single ABM simulation using realistic parameters (e.g., 13,000 neurons and 22,000+ neural connections) is an important factor in the model's usability. In this paper, we describe our efforts to improve the computational efficiency of our 3-D ABM, which resulted in a 28% reduction in execution time on average for a typical simulation. With this upgraded model, we performed one- and two-parameter sensitivity analyses to study the sensitivity of model output to variability in several key parameters along the anterior to posterior axis of the CeA. These results highlight the importance of computational modeling in exploring spatial and cell-type specific properties of brain regions to inform future wet lab experiments.

Keywords: agent-based model, amygdala, pain, sensitivity analysis, NetLogo

1 Introduction

Neuropathic pain is caused by injury or lesion to either the peripheral or central neural pathways and is characterized by both spontaneous and evoked pain [9]. After long-term injury or inflammation, substantive plasticity occurs in the central nervous system well beyond the site of injury. A variety of brain structures have been shown to be activated in this context including classic somatosensory structures (e.g., thalamus, somatosensory cortex, prefrontal cortex) as well as deeper limbic structures including the hypothalamus and amygdala.

The amygdala receives nociceptive information through several ascending pathways marking it as a central node in pain processing [3, 2, 16]. This processing includes modulation of the affective components of pain as well as behavioral adaptations to noxious sensory input (e.g., behavioral avoidance). Within the amygdala, the central nucleus of the amygdala (CeA) contains both high threshold "nociceptive" neurons as well as wide-dynamic range neurons. These neurons are largely grouped in the capsular division (CeC) of the CeA although nociceptive neurons are found in the lateral (CeL) and medial (CeM) divisions of the CeA as well. Across the CeA, neurons are heterogeneous in nature with over 20 molecular cell-types impacting the CeA's control of pain [24].

In the last decade, researchers using cell-type specific techniques coupled with optogenetics and chemogenetics have started the process of carefully dissecting the functional role of these different cell-types in pain, depression, fear-conditioning, and stress [3, 26]. In the context of nociception and pain, studies have focused on several types of cell populations characterized by expression of relatively-unique and largely non-overlapping markers. Two of the most well studied cell populations are the protein kinase c-δ (PKCδ) and somatostatin (SST) neurons.

These two cell populations are part of the GABAergic component of the CeA, which itself comprises over 65% of the neurons in the CeA [22, 13, 18]. PKCδ and SST neurons include both interneuron cells with local projections as well as those that project to a variety of CeA efferent targets including the bed nucleus of the stria terminalis (BnST), periaquaductal gray (PAG), parabrachial nucleus (PBn) and over a dozen other targets [11]. PKCδ neurons are found primarily in the CeC and CeL divisions of the CeA compared to SST neurons, which are reported to be more heavily localized to the CeL and CeM divisions [12]. While the specific areas of expression overlap, there is little overlap at the individual cell level with most reports suggesting less than 5 percent of all PKCδ and SST neurons express both cell markers [26, 12].

PKCδ and SST neurons have different impacts on pain-like behavior in rodents. In the literature, about half of the studies modulating PKCδ and SST neurons show ev-

[1]Department of Mathematics and Computer Science, Duquesne University, Pittsburgh, PA, [2]Department of Engineering, Duquesne University, Pittsburgh, PA, [3]Department of Neuroscience and Center for Advanced Pain Studies, University of Texas at Dallas, Richardson, TX

idence that PKCδ is pronociceptive (e.g., increase pain) and SST is antinociceptive (e.g., decrease pain) [26, 1]. Another set of studies has found contrasting results suggesting that some PKCδ neurons play an antinociceptive role [7] and some SST neurons play a pronociceptive role in pain [21]. This discrepancy may be related to the location of the PKCδ and SST neurons along the anterior to posterior (A→P) axis of the CeA.

Pronociceptive PKCδ neurons have been reported to likely be more anterior [1] while antinociceptive PKCδ is more posterior [7]. It should be emphasized that these generalizations for this PKCδ localized function have not been fully substantiated; this A→P hypothesis does fit into a broader data set evaluating amygdala function in a diverse set of behavioral functions including pain [4] and also appetitive behavior [10] to stress and locomotion [5]. Experimentally, evaluating the potential for A→P functional differences in the amygdala, whether for PKCδ and SST or other cell types is technically challenging given the size of the rodent CeA usually studied. Modeling of the CeA using an agent-based model (ABM) provides a computational framework to explore these hypotheses.

This paper describes our latest efforts in developing a realistic ABM of PKCδ and SST neurons to study emergent pain-related output from the CeA. In 2021, we published the first ABM describing the behaviours and interactions of PKCδ and SST neurons in the CeA and their contributions to pain. The ABM describes the firing rates, connectivity, and interactions of PKCδ and SST neurons in the left and right CeA and changes in the firing rates of these neurons attributed to neuropathic injury [14]. In the ABM, PKCδ and SST neurons are arranged in a 2-D spatial domain representing the left and right CeA, respectively, neuron firing rates are updated each time step based on laboratory data, and a network of uni-directional connections simulates the transfer of inhibitory signals between these two inhibitory neuron populations. Output from the model is a measure of pain-related output from the CeA based on the pronociceptive properties of the PKCδ neurons and antinociceptive properties of the SST neurons. A sensitivity analysis of the model showed the ratio of PKCδ to SST neurons is a key parameter in determining pain-related output. The model's predictive capabilities were tested for a range of different parameter values and output was validated with data from wet lab experiments.

In 2023, we extended this ABM framework to account for the 3-D properties of the CeA and the spatial distribution of PKCδ and SST neurons within the CeA [15]. In this latest version of the model, PKCδ and SST neurons are assigned an (x, y, z) location within a 3-D spatial domain that accurately captures the size and structural properties of the CeA. The model can be initialized with a uniform spatial distribution of PKCδ and SST neurons or a non-uniform spatial distribution based on wet lab data. The 3-D model was used to explore the impact of spatial and cell-type heterogeneity on the network properties and pain-related output from the CeA. The model also provides a framework for *in silico* testing and evaluating of spatial and cell-type specific targeting of neurons to reduce pain.

This paper focuses on improving the computational efficiency of our 3-D ABM of PKCδ and SST neurons and using the improved model to study the impact of anterior to posterior variation in key parameters on model output. In the following sections, we provide a brief overview of the 3-D ABM and discuss our efforts to reduce the model's execution time by eliminating directed links in the model's code (written in NetLogo [25]). A sensitivity analysis is performed on the model by varying key parameters in different spatial regions along the A→P axis and calculating the impact on pain-related output from the CeA.

2 Methods

2.1 Model description

Below we present a brief overview of our published 3-D agent-based model (ABM) of PKCδ and SST neurons in the central nucleus of the amygdala (CeA). The model was coded in NetLogo3D (V6.2.0) [25] and includes a graphical user interface that allows users to easily setup and execute the model. A detailed description of the ABM and its interface can be found in [15]. The NetLogo code and input files for simulating the ABM can be found in an Open Science Framework public repository (https://osf.io/t37ma/, doi: 10.17605/OSF.IO/T37MA).

2.1.1 Purpose

Our ABM simulates the behaviors and interactions of individual neurons (agents) from two distinct pain-related neuron populations in the CeA. Neurons expressing PKCδ are considered pronociceptive (i.e., increase pain) in the model while neurons expressing SST are considered antinociceptive (i.e., decrease pain) in the model. The purpose of the ABM is to synthesize laboratory data describing the location, behaviour, and connectivity of these two neuron populations into a single framework to study how these neurons work together to modulate pain-related neural activity within the CeA.

2.1.2 Spatial domain

The model's spatial domain is a realistic 3-D representation of the CeA created by exporting 3-D surface coordinates from the Blue Brain Cell Atlas [6] into NetLogo3D.

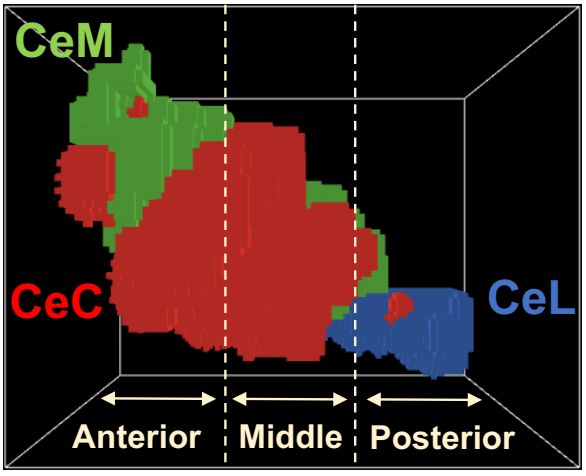

Figure 1: Spatial domain in NetLogo3D. The model's spatial domain replicates the structural properties of the CeA. Colored patches correspond to the three CeA subnuclei (CeC = red, CeM = green, CeL = blue). The x-axis denotes the anterior to posterior (A→P) axis of the brain, which was divided into three subsections (Anterior, Middle, Posterior) of equal length for our sensitivity analyses.

The spatial domain consists of 43,811 colored patches (cubes), each of which represents 25 µm × 25 µm × 25 µm. Patch color indicates whether the patch is in the lateral division (CeL = blue), medial division (CeM = green), or capsular division (CeC = red) of the CeA (Figure 1). The x-, y-, and z-axes in the spatial domain correspond to the anterior to posterior (A→P), dorsal to ventral (D→V), and lateral to medial (L→M) axes of the brain, respectively.

2.1.3 Initialization of neurons

During the model's initialization, $n = 13{,}000$ agents representing individual neurons are created and assigned a cell type (PKCδ or SST), location within the CeA, and other variables describing their behavior. The default assumption of $n = 13{,}000$ total PKCδ and SST neurons was estimated from our own laboratory experiments [15]. In Section 2.2, we explore how the total number of neurons (n) impacts the model's execution time and network properties.

The default ratio of PKCδ to SST neurons is 60:40, meaning 60% of the neurons are labeled PKCδ and 40% are labeled SST. This ratio is consistent with our own laboratory studies and others' [15, 8]. In Section 2.3.1, we perform a sensitivity analysis to determine the sensitivity of model output to the ratio of PKCδ to SST along the A→P axis.

The location of each neuron is assigned at initialization and does not change during a simulation. If the user selects 'Uniform Distribution' on the model interface, each neuron is assigned to a random patch within the CeA, resulting in a spatial distribution of PKCδ and SST neurons that is proportional to the relative volume of each CeA division. If the user selects 'Non-Uniform Distribution', each neuron is assigned to a random patch within a specific division based on wet lab data [12]. Wet lab data from [12] indicates PKCδ neurons are primarily located in the CeC and CeL whereas SST neurons are primarily located in the CeL and CeM. Table 1 displays the percentage of PKCδ and SST neurons, respectively, in each of the three divisions for the uniform and non-uniform distributions, respectively.

At initialization, each neuron is assigned three variables describing its behavior. First, each neuron has a firing frequency (Regular Spiking, Late Firing, or Spontaneous). Second, each neuron has a damage variable (d) tracking the neuron's progress towards sensitization during injury. All neurons start in the unsensitized state ($d = 0$) at initialization. During simulation, a neuron's damage level increases during periods of injury until it reaches the maximum value ($d = 100$), indicating it is fully sensitized. Lastly, each neuron has a firing rate (Fr) measured in hertz (spikes per second) that is updated each model time step.

2.1.4 Creation of network

After all neurons have been created, a network of connections is established to simulate the transmission of inhibitory signals between neurons. The model published in [15] uses directed links in NetLogo3D to represent connections between neurons. In Section 2.2, we describe the process of eliminating links from the model and using state variables to track neural connections. Both methods use the same general procedures below to establish the neural network.

To create the network, the model randomly selects a neuron (known as the transmitting neuron) and establishes a connection from this neuron to another randomly selected neuron (known as the receiving neuron) within a distance of $\text{Dist}_{\max}$ patches. This connection allows the transmitting neuron to send signals to the receiving neuron but not vice-versa. This process of creating connections between neurons repeats until all transmitting neurons have been assigned their maximum number of connections ($\text{Outgoing}_{\max}$) or no more suitable connections can be made. Parameters describing the maximum length and number of connections assigned to each transmitting neuron were determined using published connectivity data [1, 8]. These findings show PKCδ neurons have fewer primary dendrites than SST neurons, but primary

Table 1: Distribution of PKCδ and SST neurons in the CeC, CeM, and CeL sub-nuclei. Values indicate the percentage of all PKCδ and SST neurons, respectively, within each sub-nucleus. For the uniform distribution, neurons are randomly assigned a location within the CeA. For the non-uniform distribution, the percentage of neurons within each sub-nucleus was determined by laboratory data [12].

	PKCδ (%)			**SST (%)**		
	CeC	**CeL**	**CeM**	**CeC**	**CeL**	**CeM**
Uniform Dist.	37.1	17.3	45.6	37.1	17.3	45.6
Non-Uniform Dist.	49.8	44.5	5.7	6.7	51.3	42.0

dendrites extending from PKCδ neurons are typically longer than those originating from SST neurons. Consistent with the data in [1], the default parameters in our model are $\text{Outgoing}_{\max} = 1$ and $\text{Dist}_{\max} = 2.4$ patches (60 µm) for PKCδ neurons and $\text{Outgoing}_{\max} = 3$ and $\text{Dist}_{\max} = 1.6$ patches (40 µm) for SST neurons. In Section 2.3.2, we explore the sensitivity of model output to these connectivity parameters.

2.1.5 Model procedures and output

A stimulation history file describing the intensity (measured in pA) of an external stimulus during each model time step is selected by the user during initialization. For all simulations presented here, we use a ramping external stimulation in which the stimulation intensity starts at 120 pA and increases gradually to 220 pA, before returning back to 120 pA at the end of the simulation (see Figure 3A).

At the start of each time step, the model reads the stimulation intensity and updates the damage (d) and firing rate (Fr) of each neuron. Neurons accrue damage during time steps in which the external stimulus is greater than or equal to 120 pA. If a neuron's damage reaches its maximum value ($d = 100$), the neuron is considered fully sensitized. Firing rates of all neurons are updated each time step using the equation

$$Fr_i = \frac{100 - d_i}{100} \cdot X + \frac{d_i}{100} \cdot Y \tag{1}$$

where d_i is the neuron's damage level at time step i and X and Y are type-specific random variables describing the firing rates of the neuron in an unsensitized state and a sensitized state, respectively. In other words, equation (1) is a convex combination of X and Y with weights determined by the neuron's damage level. Distributions for variables X and Y in equation (1) were estimated from published physiology data [26].

After the firing rates of all PKCδ and SST neurons are updated, inhibitory signals are transmitted between neurons via the neural network. The strength of an inhibitory signal transmitted through a connection is equal to the firing rate (Fr) of the transmitting neuron. For each neuron, if the total strength of its incoming signal(s) is greater than or equal to 15 Hz ([8]), the neuron is inhibited and its firing rate is set to zero ($Fr_i = 0$). If the total strength is less than 15 Hz, the neuron's firing rate does not change.

At the end of each time step, a measure of total pain-related output (i.e., "pain") from the CeA is calculated. Pain-related output (P_i) at time i is calculated as

$$P_i = \sum_{\text{type=PKC}} \tfrac{d_i}{100} \cdot Fr_i - \sum_{\text{type=SST}} Fr_i \tag{2}$$

where d_i is a neuron's damage and Fr_i is a neuron's firing rate during time step i. In equation (2), we assume PKCδ neurons are pro-nociceptive (increase pain output) and SST neurons are anti-nociceptive (decrease pain output).

2.2 Execution time

In our previously published version of the ABM [15], we used directed links in NetLogo3D to establish the network of connections between neurons. Links are a special type of object in NetLogo3D used to represent a relationship between two agents. Directed links have built-in variables indicating the source of the link (i.e., transmitting neuron) and the destination of the link (i.e., receiving neuron).

A previous study showed that NetLogo models with a large number of links may be considerably sped up by replacing the links with state variables [20]. We implemented this strategy by creating two new state variables for each agent (neuron) in the model to track the IDs of other neurons to which they were connected. One state variable (Incoming-Connections-IDs) tracked the IDs associated with the neurons who were able to transmit signals to the agent. The second state variable (Outgoing-Connections-IDs) tracked the IDs associated with the neurons who were able to receive signals from the agent. These state variables were established for each

neuron during the model's initialization and assigned values during the creation of the network. During simulation, state variables were used each time step to determine the strength of a neuron's incoming signal. Thus, in the new version of the model, all network connections were stored in these state variables, eliminating the need for links.

To determine the impact of replacing links with state variables on our model's performance and execution time, we performed 100 replicate simulations of the model using the old version with links and another set of 100 replicate simulations using the new version with state variables. To ensure no errors were made during the conversions from links to state variables, we compared emergent output from both versions. First, the total number of connections between neurons was compared to ensure the two different network algorithms resulted in the same network sizes. Histograms were used to confirm the distributions of network sizes obtained simulations of the old and new versions of the model were similar and an unpaired t-test was applied to test for significant differences in the means of these distributions. Further, the average pain output from 100 simulations of the old and new model, respectively, were plotted and visually inspected to ensure emergent output was preserved across model versions. Finally, the execution time of each simulation was recorded and an unpaired t-test was applied to test for significant differences in the average execution time between old and new versions of the model. All analyses and comparisons were repeated using the Uniform and Non-Uniform distributions of neurons and using n = 7,000, 10,000, 13,000, and 16,000 total neurons to further study the impact of the quantity and spatial distribution of agents on network size and execution time.

All model simulations were performed on the same desktop computer equipped with an Intel i7 processor (8 Core, 16M cache, 5.1 Hz) and 16GB memory. Statistical analyses were performed using R statistical computing software [19]. In all statistical tests, we assumed $p < 0.05$ was considered statistically significant.

2.3 Sensitivity analyses

2.3.1 One-parameter sensitivity analysis

A one-parameter sensitivity analysis was performed to investigate the model's sensitivity to the ratio of PKCδ to SST neurons along the A→P axis. We first divided our model's CeA spatial domain into 'Anterior', 'Middle', and 'Posterior' regions (Figure 1). The Anterior region included CeA patches with x-coordinates ranging from 2 to 25; the Middle region included CeA patches with x-coordinates ranging from 26 to 47; and the Posterior region included CeA patches with x-coordinates ranging between 48 to 70. During model initialization, the percentage of total neurons assigned type PKCδ was varied between 30% and 90% in increments of 5% in each of the three regions one-at-a-time. The remaining neurons were assigned type SST. In other words, the PKCδ:SST ratio in each of the three regions ranged from 30:70 to 90:10 with a default ratio of 60:40.

Figure 2 shows the baseline distribution of neurons (60:40; C and D in middle row) for both the Uniform and Non-Uniform distributions and the resulting distributions when the PKCδ:SST ratio is increased to 90:10 in the Middle region only (A and B in top row) and decreased to 30:70 in the Middle region only (E and F in bottom row). When the ratio is altered in one part of the CeA (e.g., Middle region), there is no change in the other two regions and the total number of cells for the entire CeA is constant (i.e., 13,000 agents).

For each ratio explored in the Anterior, Middle, and Posterior regions, 30 replicate model simulations were executed using n = 13,000 neurons. In each simulation, we calculated the change in pain output attributed to injury (ΔP) as

$$\Delta P = P_{145} - P_{21} \tag{3}$$

where P_{145} is the pain output at time $t = 145$ (during "injury") and P_{21} is the pain output at time $t = 21$ (baseline pain; "no injury"). The average value of ΔP across the 30 replicate model simulations was plotted as a function of percent PKCδ for each of the Anterior, Middle, and Posterior regions and the slope of each was determined. A larger slope indicates a greater model sensitivity to the ratio of PKCδ to SST neurons in the respective region. We compared results from the sensitivity analysis of the model initialized with a Uniform distribution and the model initialized with a Non-Uniform distribution of neurons.

2.3.2 Two-parameter sensitivity analysis

A two-parameter sensitivity analysis was performed to study the model's sensitivity to the connectivity of PKCδ and SST neurons, respectively, along the A→P axis. The two parameters governing connectivity of a neuron in the model are the maximum number of connections assigned to a neuron ($\text{Outgoing}_{\max}$) and the maximum length of a neural connection ($\text{Dist}_{\max}$). Similar to the one-parameter sensitivity analysis, we explored the sensitivity of the model's pain output to changes in these two parameters within the Anterior, Middle, and Posterior regions of the CeA.

To investigate the impact of PKCδ connectivity on pain-related model output, the $\text{Outgoing}_{\max}$ and $\text{Dist}_{\max}$ of PKCδ neurons were varied simultaneously within each of the Anterior, Middle, and Posterior regions, while holding all other model parameters constant. In particular,

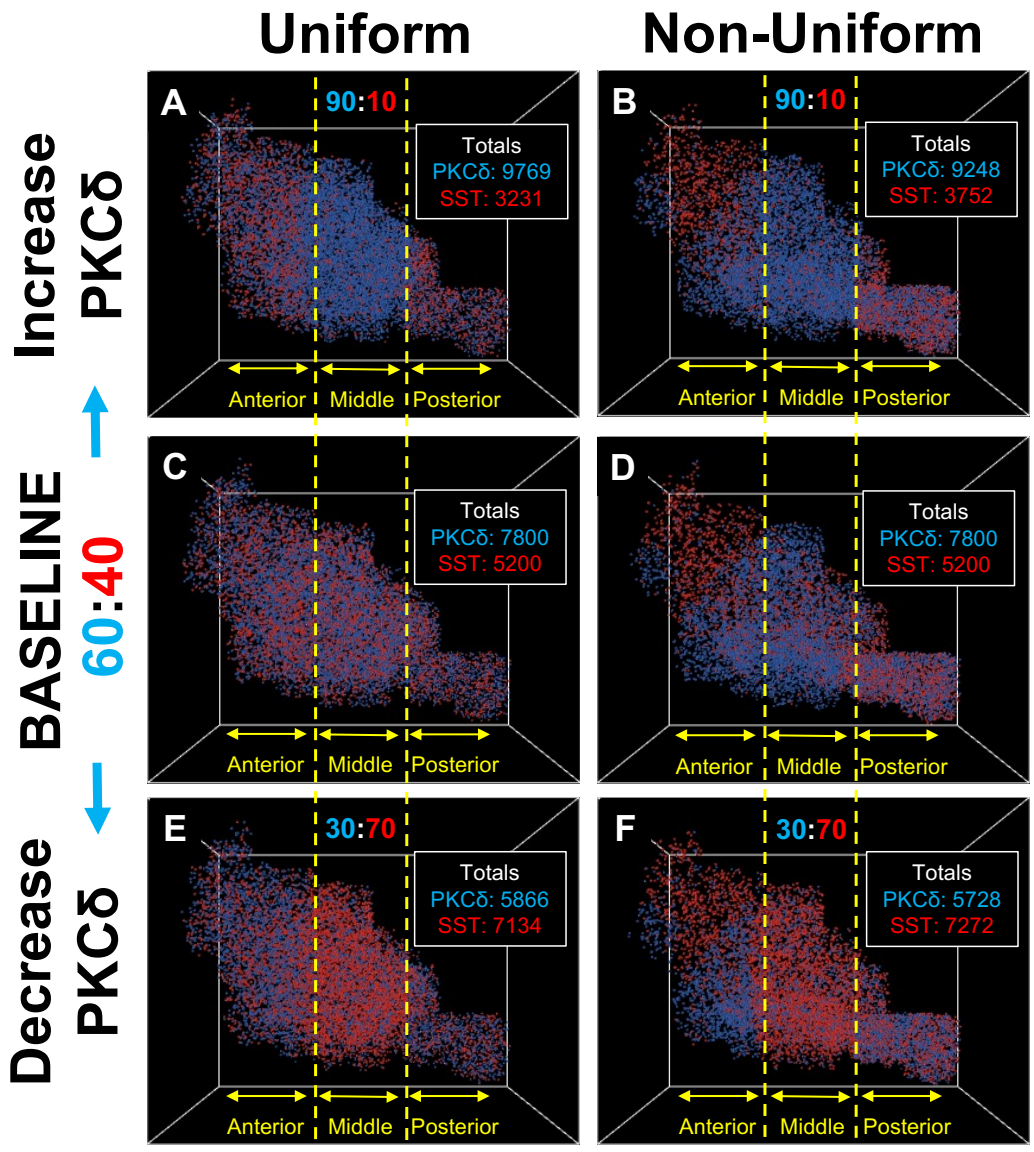

Figure 2: Variation in the PKCδ:SST ratio during one-parameter sensitivity analysis. To determine the model's sensitivity to the ratio of PKCδ to SST neurons along the A→P axis of the CeA, this ratio was varied in increments of 5% from baseline (60% PKCδ / 40% SST) within each region (Anterior, Middle, Posterior). The middle row shows the baseline distribution of neurons in the Uniform (C) and Non-Uniform (D) distributions, respectively. The top row illustrates the impact of increasing the ratio to 90:10 in the Middle region only for the Uniform (A) and Non-Uniform (B) distributions. Similarly, the bottom row illustrates the impact of decreasing the ratio to 30:70 in the Middle region only for the Uniform (E) and Non-Uniform (F) distributions.

the $\text{Outgoing}_{\max}$ of PKCδ neurons was varied between 1 and 5 connections in increments of 1, and the $\text{Dist}_{\max}$ of PKCδ neurons was varied between 1.4 patches (35 µm) and 3.4 patches (85 µm) in increments of 0.5 patches (12.5 µm). For each combination of the two parameters, 30 replicate simulations were executed and ΔP, the change in pain output attributed to injury, was calculated using equation (3). The average value of ΔP from the 30 replicate simulations was displayed in a contour plot as a multivariate function of the $\text{Outgoing}_{\max}$ and $\text{Dist}_{\max}$ for PKCδ neurons. Plots were visually inspected to assess the relationship between pain output and the connectivity of PKCδ neurons in each of the three regions (Anterior, Middle, and Posterior).

We investigated the impact of SST connectivity on pain-related output using a similar approach. Using the same procedures described above, the $\text{Outgoing}_{\max}$ of SST neurons was varied between 1 and 5 connections in increments of 1 connection, and the $\text{Dist}_{\max}$ of SST neurons was varied between 0.6 patches (15 µm) and 2.6 patches (65 µm) in increments of 0.5 patches (12.5 µm). For each parameter combination, 30 replicate simulations were performed and ΔP was calculated using equation (3). Contour plots were used to visually assess the relationship between pain output and the connectivity of SST neurons in each of the three regions.

All simulations were performed using $n = 13{,}000$ neurons and repeated for both the Uniform and Non-Uniform distributions of neurons. Contour plots were created using R statistical computing software [19].

3 Results

3.1 Replacement of links with state variables in network algorithm

The execution times of our previously published model with directed links [15] showed considerable variation based on the number of neurons; ranging from 15 seconds ($n = 7000$ neurons) to one minute or longer ($n = 16{,}000$ neurons) for a simple simulation with 385 time steps. While these times were sufficient for an initial pilot of the model, they were not ideal for performing large batches of simulations needed for sensitivity analyses. Using NetLogo's built-in `timer` primitive, we determined that a majority (50% to 70%) of the model's execution time during a single time step was spent using the network to send inhibitory signals between neurons. Therefore, in an attempt to reduce the model's execution time, we focused our efforts on redesigning how connections are established in the neural network. The computational efficiency of NetLogo models has been previously shown to improve when links are replaced with state variables [20]. The results of our study are in accordance with this finding.

The replacement of links with state variables in our network algorithm resulted in a significant decrease in execution times. Table 2 displays the average (± standard deviation) execution times (seconds) for both versions of the model for all eight scenarios. Using the old model with links, the average execution times ranged from 14.97 seconds ($n = 7{,}000$, Uniform) to 45.27 seconds ($n = 16{,}000$, Non-Uniform). Using the new model with state variables, the average execution time was less than 37 seconds for all values of n, resulting in a significant decrease in execution time across all scenarios ($p < 0.05$). All p-values are displayed in Supplemental Table S1 (see Appendix for Supplemental Tables).

Additionally, the process of eliminating links in our model and using state variables to track neural connections did not impact the model's emergent properties. Table 2 shows the average (± standard deviation) number of connections in the neural network obtained from 100 replicate simulations of the old and new model versions, respectively. As expected, as we increased the total number of neurons (n), the number of connections in the network increased proportionally for both the Uniform and Non-Uniform distributions. For each of the eight scenarios in Table 2, we found no significant difference in average number of neural connections obtained using the old version of the model with links and the new version with state variables ($p > 0.05$). All p-values are displayed in Supplemental Table S2. Histograms in Supplemental Figures S1 and S2 confirm similar distributions of total number of connections obtained using the old and new versions of the model across all eight scenarios (see Appendix for Supplemental Figures).

Similarly, both versions of the model produced the same pain output. Figure 3 shows the average value of pain output from 100 replicate simulations of the model using ramping current (Figure 3A) for both the Uniform and Non-Uniform spatial distributions of neurons. In Figure 3B, solid lines represent pain output from the old version of the model and dashed lines represent pain output from the new version. As expected, pain output is negative initially, representative of baseline conditions (no pain) prior to injury. As stimulation increases and neurons accrue damage during injury, pain output increases. Increases in pain output due to increases in stimulation are representative of evoked pain, while elevated pain levels that persist when the stimulation is decreased to 120 pA after injury are representative of spontaneous or chronic pain. For both the Uniform and Non-Uniform spatial distributions of neurons, we did not observe a difference in average pain output across the two model versions.

Table 2: Comparison of network size and execution time between new and old versions of model. Values indicate the mean (± standard deviation) of the number of connections in the neural network and the execution time (seconds) from 100 replicate simulations of the new model version (with state variables) and old model version (with links) using n = 7,000, 10,000, 13,000, and 16,000 total neurons. All simulations were repeated using the uniform and non-uniform spatial distributions of neurons. ^{ns}In all scenarios, there was no significant difference in the size of the neural network between model versions ($p \geq 0.05$). *In all scenarios, the execution time of the new model version was significantly less than the old model version ($p < 0.05$).

		Old Version of Model		**New Version of Model**	
Number of Neurons (n)	**Spatial Distribution**	**Number of Connections**	**Execution Time (s)**	**Number of Connections**	**Execution Time (s)**
7000	Uniform	9853.99 (±52.03)	14.97 (±1.85)	9850.10^{ns} (±62.48)	10.15* (±2.40)
	Non-Uniform	10099.48 (±51.12)	20.47 (±4.72)	10091.78^{ns} (±47.09)	13.29* (±3.90)
10000	Uniform	15940.76 (±53.44)	21.63 (±3.06)	15938.07^{ns} (±47.01)	14.97* (±3.34)
	Non-Uniform	15414.59 (±49.51)	27.52 (±5.71)	15410.70^{ns} (±51.94)	18.95* (±5.90)
13000	Uniform	22049.25 (±40.92)	30.01 (±4.21)	22045.73^{ns} (±41.94)	20.17* (±4.68)
	Non-Uniform	20907.94 (±53.57)	36.43 (±9.12)	20911.21^{ns} (±54.06)	26.07* (±7.55)
16000	Uniform	27958.52 (±37.73)	39.41 (±6.60)	27966.93^{ns} (±35.68)	27.05* (±5.16)
	Non-Uniform	26548.19 (±53.34)	45.27 (±11.45)	26537.59^{ns} (±50.02)	36.17* (±10.66)

3.2 Sensitivity of model output to PKCδ:SST ratio in anterior, middle, and posterior CeA

Studies have shown considerable evidence for expression differences in PKCδ to SST neurons along the A→P axis of the CeA [12, 23, 17]. Using the new model with state variables, we performed a one-parameter sensitivity analysis to investigate the model's sensitivity to the ratio of PKCδ to SST neurons along the A→P axis of the CeA. Figure 4 shows the average value of ΔP from 30 replicate model simulations plotted as a function of percent PKCδ in the Anterior, Middle, and Posterior regions, respectively. Results obtained from model simulations with the Uniform spatial distribution of neurons are displayed in Figure 4A and those from the Non-Uniform distribution are displayed in Figure 4B. It is important to note here that, throughout all simulations, the total number of neurons was held constant (n = 13,000), and, consequently, as the percent PKCδ increased from 30% to 90% within one of the three regions (Anterior, Middle, or Posterior), the percent SST decreased within the same region accordingly. Thus, values along the x-axis correspond to the ratio PKCδ:SST neurons in each region (e.g., 30% PKC indicates a 30:70 PKCδ:SST ratio).

Due to the pro-nociceptive role of PKCδ neurons in our model, increases in the percent of PKCδ neurons resulted in increases in ΔP (Figure 4). In all cases, the relationship between percent PKCδ and ΔP is linear with a positive slope (Table 3). For both the Uniform and Non-Uniform distributions, the largest slopes (m) correspond to the Middle region, indicating model output is most sensitive to PKCδ:SST ratio in the middle of the CeA. Similarly, both distributions show low to moderate sensitivity to the PKCδ:SST ratio in the Anterior region. On the other hand, the sensitivity of the model to the PKCδ:SST ratio in the Posterior varies dramatically between the two spatial distributions. Model output using a Uniform distribution of neurons is negligibly impacted by the ratio of PKCδ:SST ratio in the Posterior (m = 110.67) whereas model output using the Non-Uniform distribution of neurons is moderately sensitive to the ratio of PKCδ:SST ratio in the Posterior CeA (m = 221.39). These differences highlight the importance of accurate spatial distributions of PKCδ and SST neurons in the literature and the model.

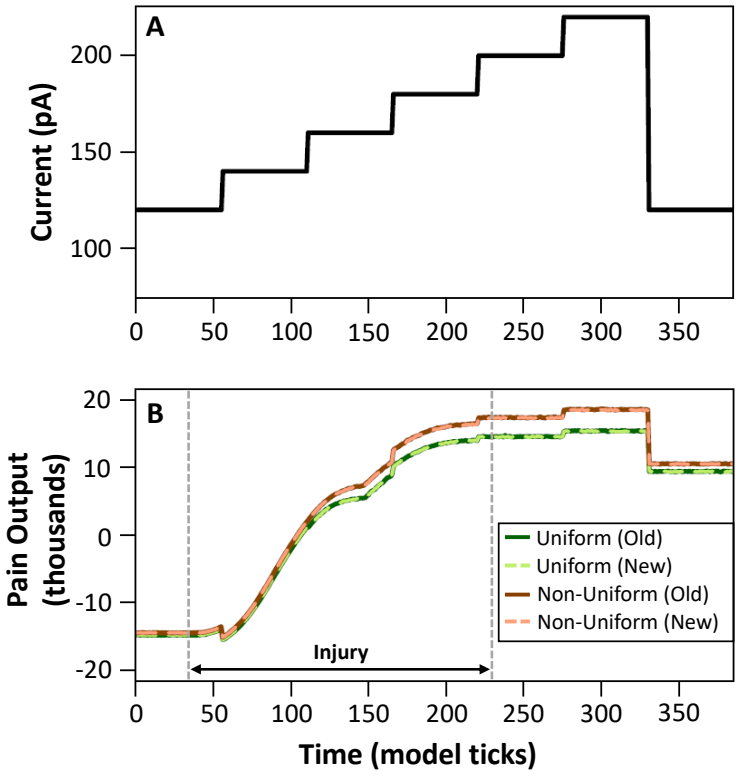

Figure 3: Comparison of pain output from the old and new versions of the model. The old model (with links) and new model (with state variables) were each simulated 100 times using the ramping current (A). Average pain output obtained from the old model (solid lines) and new model (dashed lines) is plotted in (B). Red lines represent average pain output from 100 replicate simulations using a Uniform spatial distribution of neurons. Green lines represent average pain output from 100 replicate simulations with the Non-Uniform spatial distribution of neurons (Table 1). For both spatial distributions, there is no observable difference in pain output between the old and new versions of the model.

3.3 Sensitivity of model output to neural connectivity in anterior, middle, and posterior CeA

A two-parameter sensitivity analysis was performed using the new state variable model to investigate the model's sensitivity to neural connectivity along the A→P axis. The two parameters governing the connectivity of a neuron are maximum length of connections and maximum number of connections. The relationship between pain output and the connectivity of PKCδ and SST neurons in each of the three regions (Anterior, Middle, Posterior) is displayed in Figure 5 (Uniform distribution) and Figure 6 (Non-Uniform distribution).

Contour lines in both Figure 5 and Figure 6 indicate that pain output is sensitive to the maximum number of neural connections and less so to the maximum length of connections for both SST and PKC neurons. This is visible in the large pain gradients (e.g., tightly packed contour lines) that exist in nearly all of the plots as we increase the maximum number of connections from 1 to 5 along the vertical axis. In Figure 5, we see similar pain gradients as we increase the max length of SST connections in the Anterior and Middle regions from 15 µm to 40 µm, but increases beyond 40 µm do not impact pain output reflected in the constant contour lines moving left-to-right from 40 µm.

Similar to the results of the one-parameter sensitivity analysis, the spatial distribution of neurons impacts the model's sensitivity to the connectivity parameters. Figure 5 shows the model initialized with a Uniform distribution is most sensitive to changes in SST connectivity in the Anterior and Middle regions of the model's CeA. On the other hand, Figure 6 shows the model initialized with the Non-Uniform distribution is most sensitive to changes in PKC connectivity in Middle region.

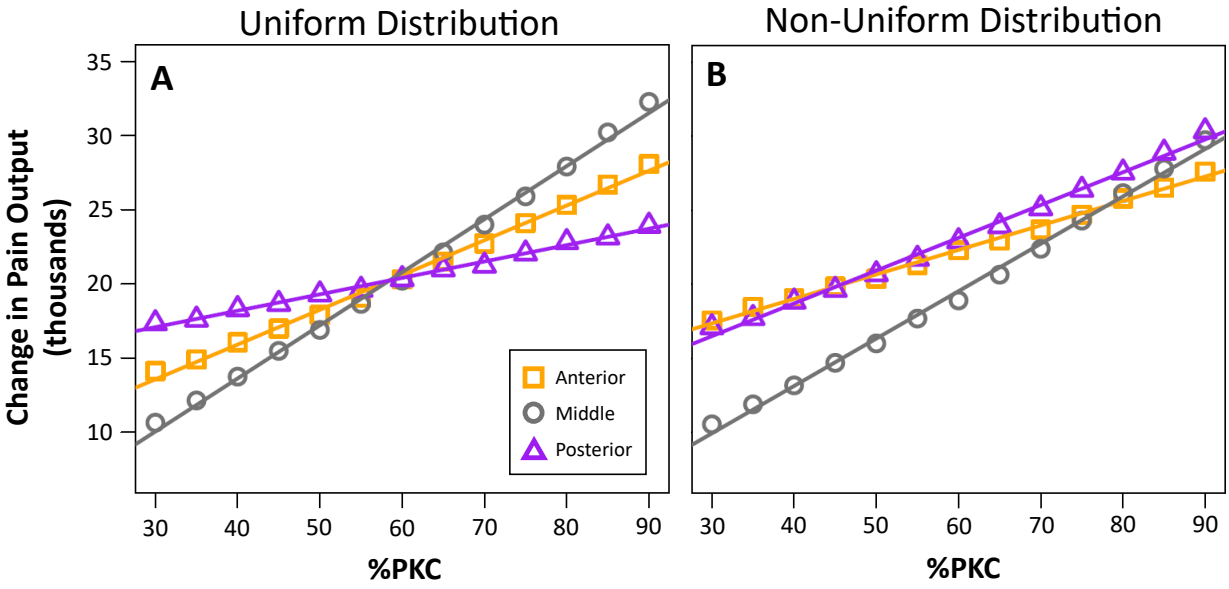

Figure 4: Sensitivity of pain output to PKCδ:SST ratio. Plots show the average change in pain attributed to injury (equation 3) from 30 simulations of the model as the percent of neurons labeled PKCδ was increased from 30% to 90% in each three CeA regions (Anterior, Middle, Posterior). As the percent PKCδ increased, the percent of neurons labeled SST decreases accordingly. For both the uniform spatial distribution (A) and non-uniform spatial distribution of neurons (B), the change in pain due to injury increases linearly as percent PKCδ increases (see Table 3).

Table 3: Regression statistics for one-parameter sensitivity analysis. The linear relationship between pain output and the percentage of neurons labeled PKCδ in each of the three regions (Anterior, Middle, Posterior) is displayed in Figure 4. For each line of best fit, the slope (m) and coefficient of correlation (R^2) is provided below. Higher slopes indicate increased model sensitivity to the parameter varied.

			Regression Statistics	
	Parameter	**Range**	**Slope (m)**	R^2
Uniform Dist.	%PKC in Anterior	$[0.3, 0.9]$	234.45	0.996
	%PKC in Middle		358.06	0.996
	%PKC in Posterior		110.67	0.994
Non-Uniform Dist.	%PKC in Anterior	[0.3, 0.9]	165.28	0.996
	%PKC in Middle		320.05	0.996
	%PKC in Poster		221.39	0.995

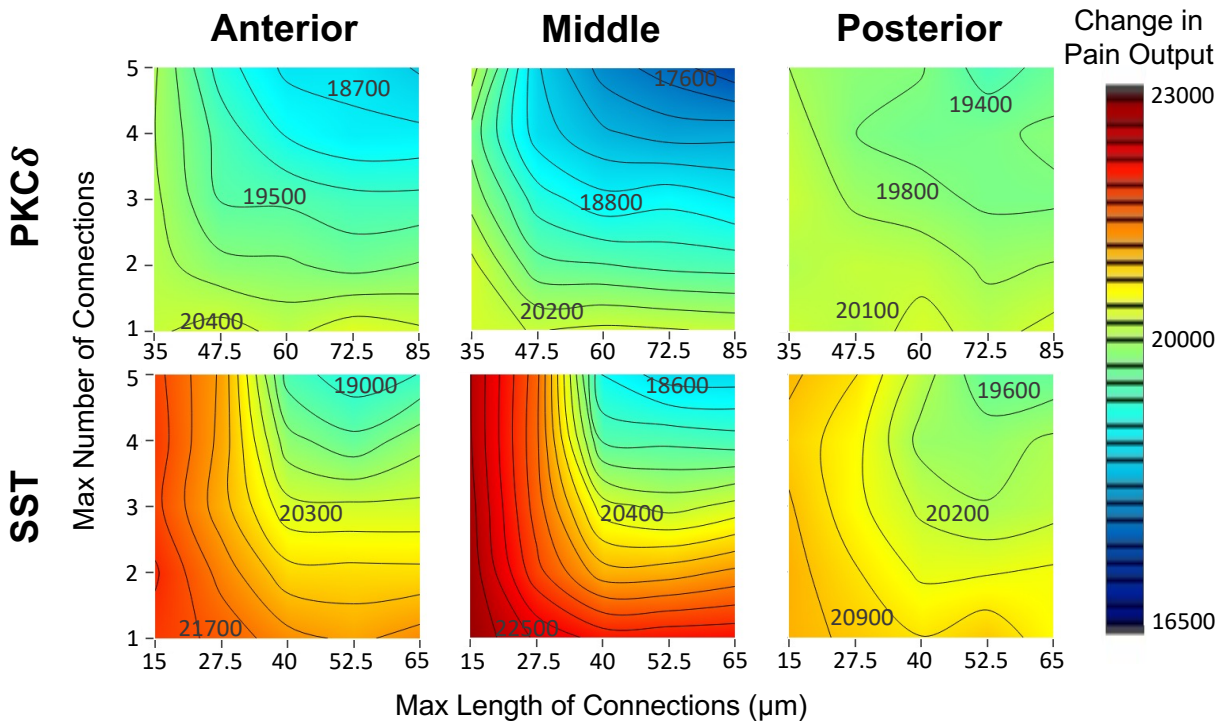

Figure 5: Sensitivity of pain output to PKCδ and SST connectivity using the Uniform distribution of neurons. Contour plots show relationship between neural connectivity and the pain output when the model is initialized with a uniform distribution of neurons. The two parameters governing neural connectivity are maximum length of connections and maximum number of connections. We varied these two parameters for PKCδ (top row) and SST (bottom row) neurons in each of the three CeA regions (Anterior, Middle, and Posterior). For each parameter combination, the model was simulated 30 times and the average change in pain attributed to injury (δP) was calculated. Results show the model initialized with a uniform distribution is most sensitive to the connectivity of SST neurons in the Anterior and Middle regions of the CeA.

4 Discussion

In this paper, we describe our efforts to reduce the execution time of our 3-D agent-based model (ABM) of PKCδ and SST neurons in the central nucleus of the amygdala (CeA). The ABM is a tool for simulating the behaviors and interactions of these two neuron populations and determining their collective contribution to pain-related output from the CeA. In a recent publication, we demonstrated the utility of the ABM in assessing the impact of spatial heterogeneity of neurons within the CeA on pain-related output and the design of spatially-targeted pain intervention methods [15]. By focusing our current efforts on reducing the execution time of the model, we aim to increase the practicality and accessibility of the model, especially to neuroscientists interested in using the model to investigate different hypotheses *in silico* before committing time and resources in the wet lab.

Similar to a previous study [20], our results show that the replacement of links in our NetLogo3D code with state variables resulted in a statistically significant reduction in execution time. Prior to implementing this change, we implemented other strategies to reduce the model's execution time, such as eliminating the re-creation of the spatial domain (CeA patches) during successive model initializations and creating global agentsets to save the IDs of agents (neurons) repeatedly called in procedures. These strategies had negligible impact on the model's execution time. In contrast, by replacing the links in the network algorithm with state variables tracking IDs of the connecting neurons, we were able to reduce the model's execution time by 28% for a typical simulation of 13,000 PKCδ and SST neurons.

A reduction in the model's execution time allowed us to efficiently perform large batches of simulations for a comprehensive sensitivity analysis of the model's parameters. Studies have shown considerable evidence for expression differences in PKCδ to SST neurons along the anterior to posterior (A$\rightarrow$P) axis of the CeA [12, 23, 17]. There-

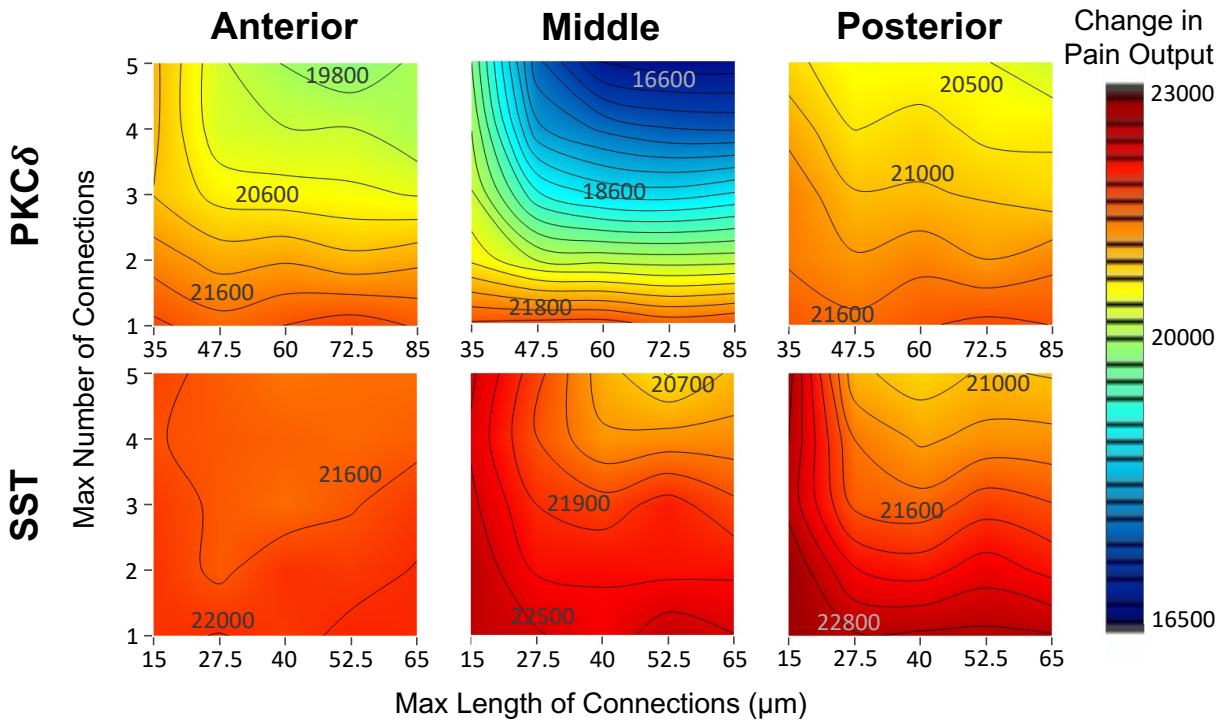

Figure 6: Sensitivity of pain output to PKCδ and SST connectivity using the Non-Uniform distribution of neurons. Contour plots show relationship between neural connectivity and the pain output when the model is initialized with the non-uniform distribution of neurons (Table 1). The two parameters governing neural connectivity are maximum length of connections and maximum number of connections. We varied these two parameters for PKCδ (top row) and SST (bottom row) neurons in each of the three CeA regions (Anterior, Middle, and Posterior). For each parameter combination, the model was simulated 30 times and the average change in pain attributed to injury (δP) was calculated. Results show the model initialized with the Non-Uniform distribution is most sensitive to the connectivity of PKCδ neurons in the Middle region of the CeA.

fore, we focused our analyses on measuring the impact of small perturbations in key parameters along the A→P axis on model predictions of pain. Sensitivity analyses can guide future wet lab studies by highlighting variables most likely to influence pain-like output in a rodent. For example, in our one-parameter sensitivity analysis, we found a significant increase in model sensitivity to the PKCδ:SST ratio in the Posterior CeA when PKCδ and SST neurons were distributed non-uniformly in the CeA using published data compared to a uniform distribution of neurons.

The one-parameter sensitivity analysis highlighted two on-going challenges in the wet lab literature. First, all currently available spatial distributions of PKCδ and SST neurons in the CeA of rodents are based on a limited sampling of the CeA across the A→P axis. Across the 1.8 mm length of the of the mouse CeA (from anterior to posterior), only six to ten 25 µm sections are typically analyzed in wet lab studies. Thus, our model has to interpolate or extrapolate parameter values in CeA regions outside of these sections. As our sensitivity analysis revealed, inaccurate parameter values in select regions of the CeA can dramatically impact model output. Second, there is a fundamental challenge in dividing the CeA into three sub-regions (whether it be Anterior, Posterior, Middle or CeC, CeM, CeL) that can ultimately lead to unintentional inaccuracy in published data. Moving forward, our results highlight the need for wet lab researchers to carefully evaluate all of the anterior-to-posterior sections in the CeA and thoughtfully consider the necessity and accuracy of sub-dividing the CeA into traditional CeC, CeL, and CeM sub-nuclei.

Our two-parameter sensitivity analysis evaluated the impact of simultaneously varying the number of connections and the length of connections for PKCδ and SST neurons. PKCδ neurons have fewer but longer connections while SST neurons have more, shorter connections [1]. The two-parameter sensitivity analysis yielded dif-

ferent results for the Uniform and Non-uniform distributions, which again highlighted the importance of the neurons' spatial distribution on model output. These results reiterate the need for accurate and consistent estimates of cell distributions for future iterations of the model. For both the Uniform and Non-uniform distributions, there was little change in model output when the length or number of connections was varied in the posterior CeA, likely due to the small size of the posterior CeA compared to the middle or anterior sections. The biggest qualitative differences between the results of the two-parameter sensitivity analysis for the Uniform and Non-uniform distributions was seen in the middle section of the CeA, which is the largest of the three sections.

The two-parameter sensitivity analysis indicated that model output is sensitive to both the number of SST connections and the length of SST connections. In nearly all cases, an increase in the number or increase in the length of SST connections led to a decrease in pain output. This result reflects the inhibitory nature of SST neurons on model output. In other words, more connections that go farther are likely to have a greater inhibitory effect. The largest variation in pain output from the two-parameter sensitivity analysis was observed in the Non-uniform model when the length and number of PKCδ connections in the middle CeA was increased. This reflects the fact that PKCδ cells in the Non-uniform model are the predominate cell population (relative to SST) in the middle region of the CeA. An increase in PKCδ connectivity in this region will then induce inhibition within the PKCδ population (i.e., PKCδ cells will inhibit other PKCδ neurons). This result points to the potential for PKCδ to provide both an anti-nociceptive and pro-nociceptive tone depending on the location of the cells within the CeA. This idea is supported by the functional experiments in the literature [24, 26, 1]. Excitingly, wet lab technological improvements with viral targeting now provide opportunities to explore such A→P functional differences in future whole animal experiments.

Data Availability Statement

All NetLogo3D code and supporting files for implementing the ABM are available in a public repository. Readers may find it at https://osf.io/t37ma/.

Acknowledgments

This work was supported through NIH research grants R15NS128624 (PI Neilan) and R01DK115478 (PI Kolber).

Author Contributions

Kayla Kraeuter (undergraduate student) updated the ABM as described in this paper and performed all model simulations and analyses presented here. Carley Reith (undergraduate student) developed the original version of the ABM published in [15]. Rachael Miller Neilan (faculty) and Benedict Kolber (faculty) oversaw the development of the ABM, estimation of parameter values, and interpretation of results. All authors contributed to the writing of this paper.

References

[1] Adke, A. P., Khan, A., Ahn, H. S., Becker, J. J., Wilson, T. D., Valdivia, S., Sugimura, Y. K., Martinez Gonzalez, S., and Carrasquillo, Y. (2020). Cell-type specificity of neuronal excitablity and morphology in the central amygdala. *eNeuro*, 8(1):1–28.

[2] Allen, H. N., Bobnar, H. J., and Kolber, B. J. (2021). Left and right hemispheric lateralization of the amygdala in pain. *Prog Neurobiol*, 196:101891

[3] Allen, H. N., Chaudhry, S., Hong, V. M., Lewter, L. A., Sinha, G. P., Carrasquillo, Y., Taylor, B. K., and Kolber, B. J. (2023). A Parabrachial-to-Amygdala Circuit That Determines Hemispheric Lateralization of Somatosensory Processing. *Biol Psychiatry*, 93(4):370–381.

[4] Bowen, A. J., Huang, Y. W., Chen, J. Y., Pauli, J. L., Campos, C. A., and Palmiter, R. D. (2023). Topographic representation of current and future threats in the mouse nociceptive amygdala. *Nat Commun*, 14(196).

[5] Coover, G. D., Murison, R., and Jellestad, F. K. (1992). Subtotal lesions of the amygdala: the rostral central nucleus in passive avoidance and ulceration. *Physiol Behav*, 51(4):795–803.

[6] Erö, C., Gewaltig, M. O., Keller, D., and Markram, H. (2018). A cell atlas for the mouse brain. *Frontiers in Neuroinformatics*, 12:84.

[7] Hua, T., Chen, B., Lu, D., Sakurai, K., Zhao, S., Han, B. X., Kim, J., Yin, L., Chen, Y., Lu, J., and Wang, F. (2020). General anesthetics activate a potent central pain-suppression circuit in the amygdala. *Nat Neurosci*, 23(7):854–868.

[8] Hunt, S., Sun, Y., Kucukdereli, H., Klein, R., and Sah, P. (2017). Intrinsic circuits in the lateral central amygdala. *eNeuro*, 4(1):1–18.

[9] International Association for the Study of Pain. Pain Terms. https://www.iasp-pain.org/resources/terminology/

[10] Kim, J., Zhang, X., Muralidhar, S., LeBlanc, S. A., and Tonegawa, S. (2017). Basolateral to Central Amygdala Neural Circuits for Appetitive Behaviors. *Neuron*, 93(6):1464–1479.e5.

[11] Liu, J., Hu, T., Zhang, M. Q., Xu, C. Y., Yuan, M. Y., and Li, R. X. (2021). Differential efferent projections of GABAergic neurons in the basolateral and central nucleus of amygdala in mice. *Neurosci Lett*, 745:135621.

[12] McCullough, K. M., Morrison, F. G., Hartmann, J., Carlezon, W. A., Jr., and Ressler, K. J. (2018). Quantified coexpression analysis of central amygdala subpopulations. *eNeuro*, 5(1):1–12.

[13] McDonald, A. J. and Augustine, J. R. (1993). Localization of GABA-like immunoreactivity in the monkey amygdala. *Neuroscience*, 52(2): 281–94.

[14] Miller Neilan, R., Majetic, G., Gil-Silva, M., Adke, A. P., Carrasquillo, Y., and Kolber, B. J. (2021). Agent-based modeling of the central amygdala and pain using cell-type specific physiological parameters. *PLOS Computational Biology*, 17(6):e1009097.

[15] Miller Neilan, R., Reith, C., Anandan, I., Kraeuter, K., Allen, H. N., and Kolber, B. J. (2023). Developing a 3-D computational model of neurons in the central amygdala to understand pharmacological targets for pain. *Frontiers in Pain Research*, 4 (1183553).

[16] Neugebauer, V., Mazzitelli, M., Cragg, B., Ji, G., Navratilova, E., and Porreca, F. (2020). Amygdala, neuropeptides, and chronic pain-related affective behaviors. *Neuropharmacology*, 170:108052.

[17] O'Leary, T. P., Kendrick, R. M., Bristow, B. N., Sullivan, K. E., Wang, L., Clements, J., Lemire, A. L., and Cembrowski, M. S. (2022). Neuronal cell types, projections, and spatial organization of the central amygdala. *iScience* 25:105497.

[18] Paré, D. and Smith, Y. (1993). Distribution of GABA immunoreactivity in the amygdaloid complex of the cat. *Neuroscience*, 57(4): 1061–76.

[19] R Core Team (2016). R: A language and environment for statistical computing. Vienna, Austria: R Foundation for Statistical Computing.

[20] Railsback, S., Ayllón, D., Berger, U., Grimm, V., Lytinen, S., Sheppard, C., and Thiele, J. (2017). Improving execution speed of models implemented in NetLogo. *Journal of Artificial Societies and Social Simulation*, 20(1):3.

[21] Raver, C., Uddin, O., Ji, Y., Li, Y., Cramer, N., Jenne, C., Morales, M., Masri, R., and Keller, A. (2020). An Amygdalo-Parabrachial Pathway Regulates Pain Perception and Chronic Pain. *J Neurosci*, 40(17):3424–3442.

[22] Rodarie, D., Verasztó, C., Roussel, Y., Reimann, M., Keller, D., Ramaswamy, S., Markram, H., and Gewaltig, M. (2022). A method to estimate the cellular composition of the mouse brain fro heterogeneous datasets. *PLOS Computational Biology*, 18(12): e1010739.

[23] Wang, A., Krabbe, S., Eddison, M., Henry, F.E., Fleishman, G., Lemire, A.L., Wang, L., Korff, W., Tillberg, P.W., Lüthi, A., and Sternson, S.M. (2023). Multimodal mapping of cell types and projections in the central nucleus of the amygdala. *eLife*, 12:e84262.

[24] Wang, Y., Krabbe, S., Eddison, M., Henry, F. E., Fleishman, G., Lemire, A. L., Wang, L., Korff, W., Tillberg, P. W., Luthi, A., and Sternson, S. M. (2023). Multimodal mapping of cell types and projections in the central nucleus of the amygdala. *eLife*, 12:e84262.

[25] Wilensky, U. (1999). *NetLogo and NetLogo 3D* Center for Connected Learning and Computer-Based Modeling, Northwestern University, Evanston, IL.

[26] Wilson, T. D., Valdivia, S., Khan, A., Ahn, H. S., Adke, A. P., Martinez Gonzalez, S., Sugimura, Y. K., and Carrasquillo, Y. (2019). Dual and opposing functions of the central amygdala in the modulation of pain. *Cell Reports*, 29(2):332–346e5.

Appendix

Table S1: Comparison of execution time between new and old versions of model. Values indicate the mean (± standard deviation) of the execution time (seconds) from 100 replicate simulations of the new model version (with state variables) and old model version (with links) using n = 7,000, 10,000, 13,000, and 16,000 total neurons. All simulations were repeated using the uniform and non-uniform spatial distributions of neurons. An unpaired t-test was applied to test for a significant difference in the mean execution time of corresponding simulations from the new and old versions of the model. The resulting p-values are displayed here. *In all scenarios, the execution time of the new model version was significantly less than the old model version ($p < 0.05$).

Number of Neurons (n)	**Spatial Distribution**	**Old Version of Model Execution Time (s)**	**New Version of Model Execution Time (s)**	**p-value**
7000	Uniform	14.97 (±1.85)	10.15* (±2.40)	1.68×10^{-36}
	Non-Uniform	20.47 (±4.72)	13.29* (±3.90)	2.73×10^{-24}
10000	Uniform	21.63 (±3.06)	14.97* (±3.34)	1.81×10^{-33}
	Non-Uniform	27.52 (±5.71)	18.95* (±5.90)	1.28×10^{-20}
13000	Uniform	30.01 (±4.21)	20.17* (±4.68)	2.87×10^{-36}
	Non-Uniform	36.43 (±9.12)	26.07* (±7.55)	1.07×10^{-15}
16000	Uniform	39.41 (±6.60)	27.05* (±5.16)	3.49×10^{-33}
	Non-Uniform	45.27 (±11.45)	36.17* (±10.66)	2.42×10^{-8}

Table S2: Comparison of network size between new and old versions of model. Values indicate the mean (± standard deviation) of the number of connections in the neural network from 100 replicate simulations of the new model version (with state variables) and old model version (with links) using n = 7,000, 10,000, 13,000, and 16,000 total neurons. All simulations were repeated using the uniform and non-uniform spatial distributions of neurons. An unpaired t-test was applied to test for a significant difference in the mean network size of corresponding simulations from the new and old versions of the model. The resulting p-values are displayed here. ^{ns}In all scenarios, there was no significant difference in the size of the neural network between model versions ($p \geq 0.05$).

Number of Neurons (n)	**Spatial Distribution**	**Old Version of Model Number of Connections**	**New Version of Model Execution Time (s)**	**p-value**
7000	Uniform	9853.99 (±52.03)	9850.10^{ns} (±62.48)	0.63
	Non-Uniform	10099.48 (±51.12)	10091.78^{ns} (±47.09)	0.27
10000	Uniform	15940.76 (±53.44)	15938.07^{ns} (±47.01)	0.71
	Non-Uniform	15414.59 (±49.51)	15410.70^{ns} (±51.94)	0.59
13000	Uniform	22049.25 (±40.92)	22045.73^{ns} (±41.94)	0.55
	Non-Uniform	20907.94 (±53.57)	20911.21^{ns} (±54.06)	0.67
16000	Uniform	27958.52 (±37.73)	27966.93^{ns} (±35.68)	0.11
	Non-Uniform	26548.19 (±53.34)	26537.59^{ns} (±50.02)	0.15

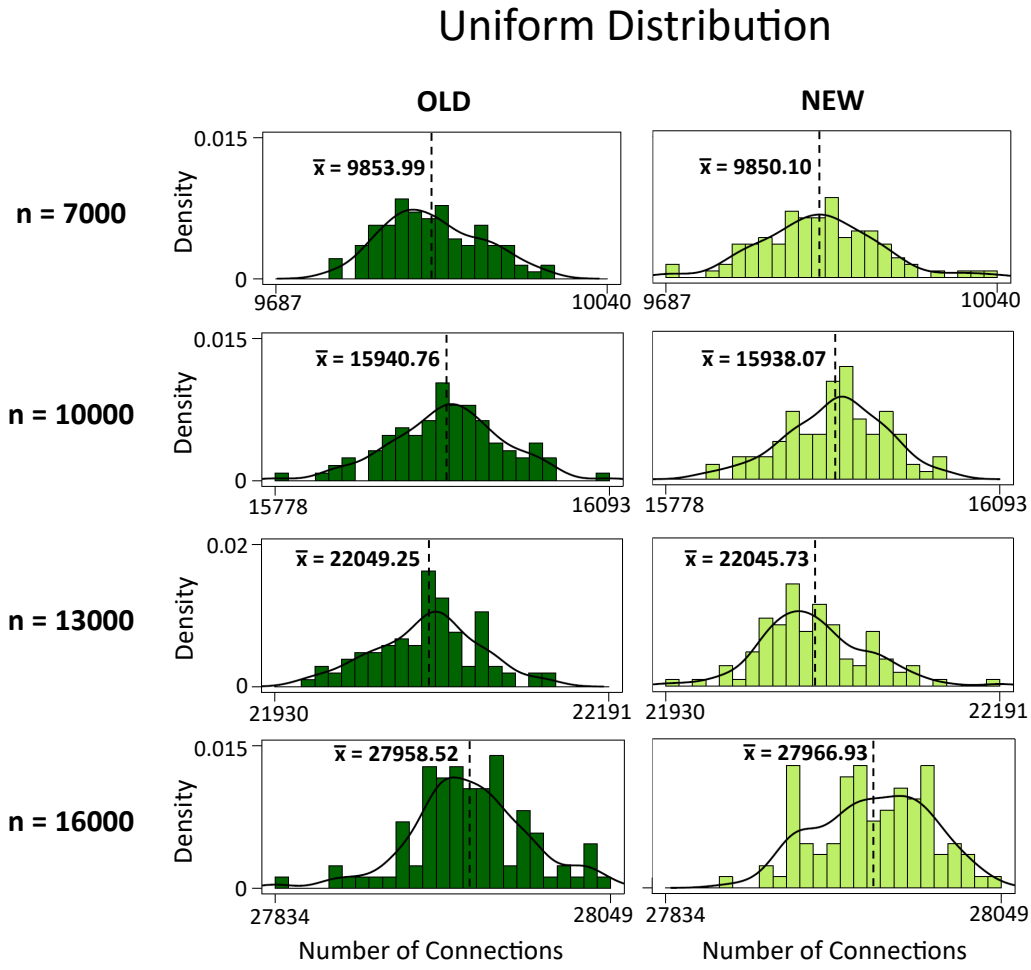

Figure S1: Comparison of the number of connections generated from old and new versions of the model using a Uniform spatial distribution of neurons. Histograms display the total number of connections obtained from 100 replicate simulations of the model initialized with using $n = 7{,}000$, 10,000, 13,000, 16,000 total neurons and a Uniform spatial distribution of neurons. Distributions obtained from the old version of the model (left column) are similar to those obtained from the new version of the model (right column). In all scenarios, there is no significant difference in the average number of connections ($\bar{x}$) between the two model versions ($p > 0.05$, Table 2).

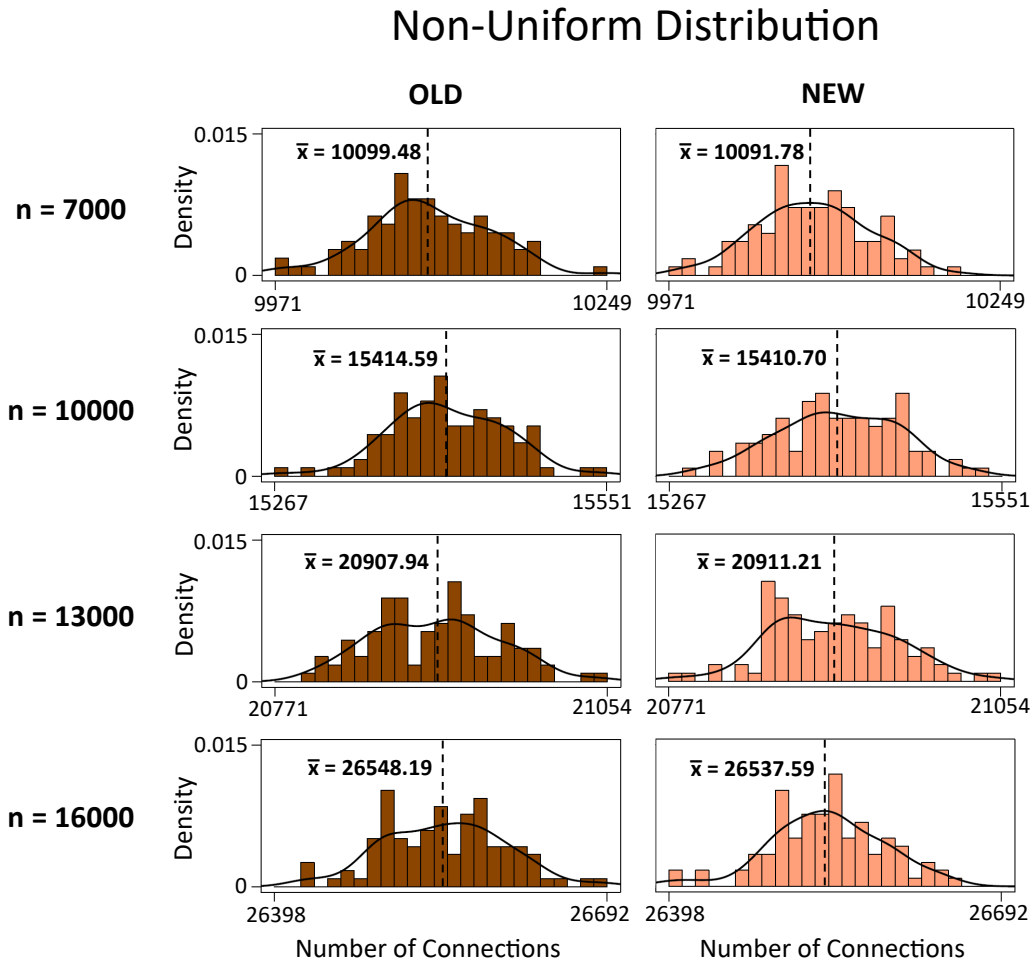

Figure S2: Comparison of the number of connections generated from old and new versions of the model using the Non-Uniform spatial distribution of neurons. Histograms display the total number of connections obtained from 100 replicate simulations of the model initialized with using $n = 7{,}000$, 10,000, 13,000, 16,000 total neurons and the Non-Uniform spatial distribution of neurons (Table 1). Distributions obtained from the old version of the model (left column) are similar to those obtained from the new version of the model (right column). In all scenarios, there is no significant difference in the average number of connections ($\bar{x}$) between the two model versions ($p > 0.05$, Table 2).